JGR Solid Earth

RESEARCH ARTICLE
10.1029/2020JB020019

Key Points:

- Weak intensity of Cretaceous and Paleogene stable magnetic field
- Variable vertical-axis block-rotations in adjacent zones accommodated continental collision
- Multimethod approach increases reliability of paleointensity determinations

Supporting Information:

- Supporting Information S1

Correspondence to:
M. Calvo-Rathert,
mcalvo@ubu.es

Citation:
Calvo-Rathert, M., Bógalo, M. F., Morales, J., Goguitchaichvili, A., Lebedev, V. A., Vashakidze, G., et al. (2021). An integrated paleomagnetic, multimethod-paleointensity, and radiometric study on Cretaceous and Paleogene lavas from the Lesser Caucasus: Geomagnetic and tectonic implications. *Journal of Geophysical Research: Solid Earth*, *126*, e2020JB020019. https://doi.org/10.1029/2020JB020019

Received 20 APR 2020
Accepted 23 NOV 2020

An Integrated Paleomagnetic, Multimethod-Paleointensity, and Radiometric Study on Cretaceous and Paleogene Lavas From the Lesser Caucasus: Geomagnetic and Tectonic Implications

M. Calvo-Rathert[1,2], M. F. Bógalo[1], J. Morales[3], A. Goguitchaichvili[3], V. A. Lebedev[4], G. Vashakidze[5], N. García-Redondo[1], and E. Herrero-Bervera[2]

[1]Departamento de Física, EPS, Universidad de Burgos, Burgos, Spain, [2]Hawaii Institute of Geophysics and Planetology, SOEST, University of Hawaii at Manoa, Honolulu, HI, USA, [3]Laboratorio Interinstitucional de Magnetismo Natural, Instituto de Geofísica Unidad Michoacán, UNAM, Morelia, Mexico, [4]Institute of Geology of Ore Deposits, Petrography, Mineralogy and Geochemistry—Russian Academy of Sciences (IGEM RAS), Moscow, Russia, [5]Alexandre Janelidze Institute of Geology—Ivane Javakhishvili Tbilisi State University, Tbilisi, Georgia

Abstract Sixteen rhyolitic and dacitic Cretaceous and Paleocene-Eocene lavas from the Lesser Caucasus have been subjected to paleomagnetic and multimethod paleointensity experiments to analyze the variations of the Earth's magnetic field. Paleointensity experiments were performed with two methods. Thellier-type experiments with the IZZI method on 65 specimens (nine flows) yielded 15 successful determinations and experiments with the multispecimen method on 14 samples (seven flows) yielded two successful determinations. The joint analysis of the results obtained with both methods produced a mean $F_{uK} = (19.9 \pm 3.7)$ μT for upper Cretaceous and $F_{Pg} = (20.7 \pm 3.3)$ μT for Paleogene sites. Low virtual axial dipole moments for the Cretaceous (3.4×10^{22} Am^2) and Paleogene (3.5×10^{22} Am^2) samples support the idea of a lower average dipole moment during periods of stable polarity of the Earth magnetic field. Mean flow paleomagnetic directions did not match expected upper Cretaceous to Paleogene directions calculated from the European *Apparent Polar Wander Path*. While inclination results roughly agreed with expected values, a group of sites showed nearly North-South paleodeclinations ($D = 1.1° \pm 14.2°$), and another group displayed eastward deviated paleodeclinations ($D = 72.9° \pm 26.6°$). These results suggest the occurrence of nearly vertical-axis rotations, probably as a result of continental collision since Oligocene. In addition to paleomagnetic and palaeointensity analyses, new K-Ar absolute age determinations have been performed on three of the studied sites, yielding Late Cretaceous ages (78.7 ± 1.7, 79.7 ± 1.6, and 83.4 ± 1.8 Ma (2σ)).

Plain Language Summary Paleomagnetic and paleointensity experiments allow the retrieval of the intensity and direction of the magnetic field of the Earth (EMF) in the geological past, so that this kind of data can inform us about how the EMF has changed with time. Furthermore, paleomagnetic directions can also inform us about what kind of tectonic movements the studied regions have experienced. If the experimental results obtained do not agree with known expected directions, this can be an indication of tectonic movements in the study area. In the present study, we have analyzed rocks with ages between ~50 and 85 million years. Analysis of their paleointensity suggests that the strength of the EMF at that time could have been lower than half its present-day value. The study of the magnetization directions recorded in these rocks tells us that the study region has been deformed experiencing rotations of different magnitudes in adjacent areas, as a result of the collision of the Eurasian and Arabian plates. Furthermore, we have obtained three new absolute age data for the analyzed rocks.

1. Introduction

Paleomagnetic and paleointensity data can supply evidence about the past characteristics and fluctuations of the geomagnetic field. Such information provides constraints which contribute to an improved knowledge of the processes taking place in the deep interior of the Earth (e.g., Biggin & Paterson, 2015). When a rock is magnetized in the Earth's magnetic field (EMF), its remanence vector is generally (nearly) parallel to the latter. Thus, information about directional EMF variations can be in principle directly determined

from the remanence vector obtained in paleomagnetic analyses. Nevertheless, the attainment of a more comprehensive image of the past EMF requires the knowledge of the full field vector. Absolute paleointensity determinations, however, are rather complex, as this magnitude is not only related to the intensity of the magnetizing field but can also be strongly influenced by the magnetic properties of the field recording minerals.

Because of the experimental and intrinsic difficulties of paleointensity determinations, failure rates can be rather large. In fact, in Thellier-type experiments (Thellier & Thellier, 1959), which are regarded the most trustworthy because they rely on a robust physical basis, several requirements have to be fulfilled by the analyzed samples in order to deliver reliable paleointensity determinations: (i) remanent magnetization must be of thermal origin, i.e., a thermoremanent magnetization (TRM); (ii) samples must comply with the so-called Thellier laws (Thellier & Thellier, 1959), a requisite which is only rigorously met by noninteracting single-domain (SD) grains (e.g., Dunlop, 2011, and references therein); and (iii) magnetic phases should not experience physical, mineralogical, or chemical alterations during heating, as this can lead to spurious paleointensity estimates. In some cases, apparently reliable determinations may produce erroneous paleointensity results (e.g., Calvo et al., 2002; Draeger et al., 2006; Gribov et al., 2019; Shcherbakov et al., 2019; Smirnov & Tarduno, 2005). As revealed by the paleointensity database PINT2015.05 (Biggin et al., 2009, 2010), this has led to a relative scarcity of paleointensity data which in addition are both temporarily and geographically unevenly distributed. Available paleointensity data so far are strongly concentrated toward the youngest periods. However, a better understanding of the geodynamo entails a deeper knowledge of the behavior of the EMF with time, including not only the variations of its direction, but also of its intensity. The Cretaceous period is especially interesting due to the occurrence of a long period of normal polarity, lasting from ~121 to 83 million years ago (Cande & Kent, 1995; He et al., 2008; Prévot et al., 1990). Subsequently, the reversal rate of the geomagnetic field started to rise. A weak correspondence between reversal frequency and intensity of the EMF has been proposed (Constable et al., 1998; Kulakov et al., 2019), but a still relatively limited amount of diverging paleointensity results has been obtained for the late Cretaceous period (PINT database, Biggin et al., 2010).

Some new paleointensity determination techniques have been put forward to avoid or reduce the impact of the presence of multidomain (MD) grains and the occurrence of chemical and/or mineralogical alterations in the studied samples (e.g., Dekkers & Böhnel, 2006; Walton et al., 1992). Based on a theoretical model proposed by Biggin and Poidras (2006), the multispecimen (MS) method was developed by Dekkers and Böhnel (2006). In this method, several specimens are taken from a sample or near lying points of a volcanic flow or an archeological object. Then, a partial TRM (pTRM) is imparted to each specimen parallel to its natural remanent magnetization (NRM), choosing different laboratory fields but keeping the same temperature. When the sum of this pTRM and the specimen's remaining magnetization matches the value of the original NRM, the field generating the pTRM is assumed to have the intensity of the primary magnetizing field. As the field is imparted parallel to the specimens' NRM and eliminates magnetic history effects, paleointensity determination should not depend on domain structure. Moreover, the possibility of alteration would be also diminished, as specimens only experience a single heating with a heating temperature that is chosen such as to avoid significant alterations, while still de/remagnetizing a meaningful proportion of the full remanence of each specimen. This method was, however, questioned by Fabian and Leonhardt (2010), who argued that the presence of MD grains could deliver systematic paleointensity overestimates. In fact, paleointensity overestimates with the MS method have been described by Michalk et al. (2008, 2010) and Calvo-Rathert et al. (2016). Fabian and Leonhardt (2010) put forward a new theoretical model and proposed a new MS measurement protocol including extra correction steps to prevent these overestimates.

Different experimental procedures of paleointensity determination are based on reaching different states of energy equilibrium, which depend on applied fields, temperature or the demagnetizing field at every heating step. Consequently, the reliability of paleointensity determinations can be enhanced by considering the agreement of results arising from methods based on a different physical basis (e.g., Böhnel et al., 2009; Calvo-Rathert et al., 2016, 2019; De Groot et al., 2013, 2015; Enterpinar et al., 2016; Monster et al., 2015a, 2018).

Due to its location in the Arabia-Anatolia-Eurasia collision zone, the Caucasus region is characterized by a complex tectonic history (e.g., Adamia et al., 2011; Rolland, 2017). During the last 3 decades, a number of new paleointensity and paleomagnetic studies have been performed in the Caucasus area employing

modern methods and being accessible in international journals (Asanidze et al., 2009; Bazhenov & Burtman, 2002; Bazhenov et al., 1996; Caccavari et al., 2014; Calvo-Rathert et al., 2008, 2011, 2013, 2015; Camps et al., 1996; Goguitchaichvili & Parès, 2000; Goguitchaichvili et al., 1997, 2000, 2001, 2009, 2016; Meijers et al., 2015; Sánchez-Moreno et al., 2018a, 2020; Shcherbakova et al., 2007, 2009). Most of these investigations, however, have been carried out on Pliocene and Pleistocene rocks, mainly from the Javakheti Highland. Only five of the aforementioned studies have been performed on older rocks: Miocene to upper Cretaceous (Meijers et al., 2015), middle Eocene (Bazhenov & Burtman, 2002), upper Cretaceous (Asanidze et al., 2009; Shcherbakova et al., 2007), and lower and middle Jurassic (Bazhenov et al., 1996). Merely the study of Shcherbakova et al. (2007) includes paleointensity determinations.

The main goal of the present study is to obtain new paleomagnetic directional and paleointensity information for the still limited Upper Cretaceous to Paleogene database in the Caucasus region together with new radiometric age data.

2. Geological Context, Sampling, and K-Ar Ages

The Caucasus region belongs to the Alpine-Himalayan orogenic belt and its geological and tectonic history is the result of the interplay of the still-converging African-Arabian and Eurasian plates (e.g., Adamia et al., 2011). From the Late Paleozoic to the Early Cenozoic, the Caucasus region was part of the Tethys Ocean and its Gondwanan (African-Arabian) and Eurasian margins. During the Late Paleozoic-Early Cenozoic precollisional stage, a system of island-arcs, intraarc rifts and back-arc basins was formed. In the Greater and Lesser Caucasus, back-arc basins were inverted to fold-thrust belts due to the continuing African-Arabian and Eurasian convergence during Oligocene-Middle Miocene (syn-collisional stage) and Late Miocene-Quaternary (postcollisional stage) (Adamia et al., 2011). The position of the Caucasus region between the two plates converging at a ∼20–30 mm/year (Adamia et al., 2011) rate determines its recent geodynamics and complex active tectonics. In Georgia, the nearly N-S compression due to the convergence of the Eurasian and African-Arabian plates generates three main directions of active faults (Koçyiğit et al., 2001). One group includes faults with a WNW-ESE or W-E strike related to compressional structures. In the remaining two groups, faults show either a NW-SE or a NE-SW strike and are mainly related to extensional structures with a substantial strike-slip component (Adamia et al., 2011).

The study area lies in the region around the Bolnisi district in Georgia, located ∼60 km SW of Tbilisi (Figure 1). The Bolnisi area belongs to the Artvin-Bolnisi unit, which is one of the tectonic units or terrains into which the Caucasus is divided. From Late Jurassic to Paleogene, the Artvin-Bolnisi unit formed part of a volcanic arc complex on the southern margin of the Eurasian plate together with the Adjara-Trialeti unit to the north and the Bayburth-Karabakh imbricated unit to the south. Between Aptian-Albian to Campanian, widespread volcanic activity took place in the Artvin-Bolnisi unit (e.g., Yilmaz et al., 2000). The volcanic units are formed by basalts, andesite, dacite, and rhyolite (lavas and pyroclastics), with a thickness reaching 3,000–4,000 m (Adamia et al., 2011). In some localities of the Artvin–Bolnisi unit, Paleocene to Eocene lavas and pyroclastics of different composition with a thickness of 100–300 m can be found (Adamia et al., 2011; Aydinçakir & Sen, 2013) related to basaltic troughs formed in that period (Lordkipanidze et al., 1989). In the Artvin-Bolnisi unit, Cretaceous volcanic sequences are cut in many places by numerous hypabyssal and plutonic bodies of Late Cretaceous and Paleogene age with predominance of rocks of acid composition.

In order to perform a paleomagnetic and paleointensity study, 168 cores were taken from 16 ryolithic and dacitic volcanics (Table 1 and Figure 1) of Paleogene and Cretaceous age in the Bolnisi district in the Republic of Georgia. Samples were taken with a portable drill and cores were oriented with a Pomeroy orientation device and both a magnetic and a solar compass.

K-Ar age determinations were performed on samples of three of the studied sites in the Isotope laboratory of the Institute of Geology of Ore Deposits, Petrography and Geochemistry of the Russian Academy of Sciences in Moscow (Table S1). The preparation procedure for samples included crushing of the rocks in steel mortar, sieving (the fraction with grain size 0.25–0.50 mm was picked out), washing in distilled water, and drying at a temperature below 50 °C. The separated groundmass and biotite preparations were used for dating. The potassium contents were determined twice by the flame photometry method using an FPA-01 spectrometer (Elam-Center). Radiogenic argon content analyses were carried out twice on an MI-1201 IG

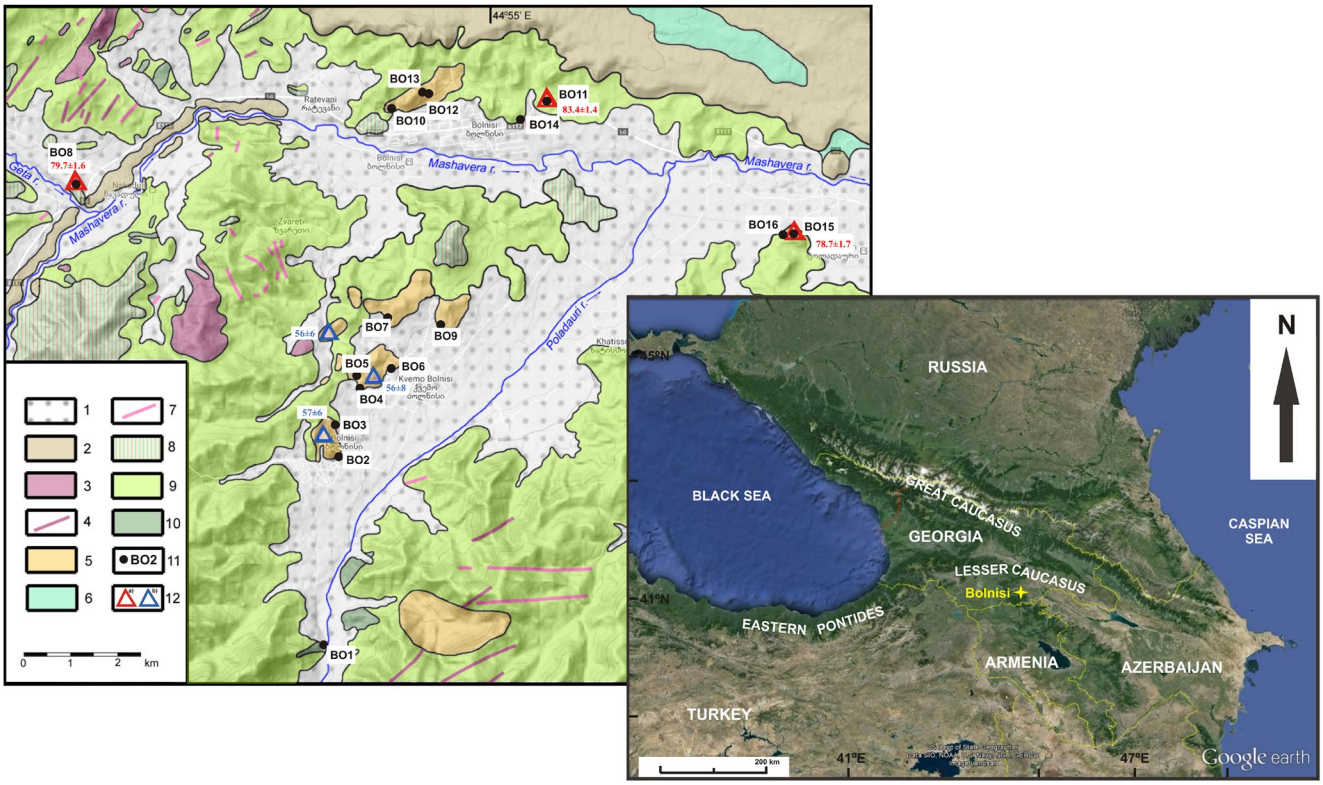

Figure 1. Study area. (a) Map of the Caucasus and adjacent regions. Study area is marked by a red star. Adapted from Google Earth; (b) *Geological map of the Bolnisi area*. Modified from Adamia et al. (1960). 1—Quaternary sediments; 2—Neogene-Quaternary basalts and basaltic andesites of Mashavera and Khrami lava flows; 3—small intrusions of Eocene granodiorites; 4—dikes of Eocene granodiorites and diorites; 5—hypabyssal bodies of Paleocene-Eocene rhyolites, dacites, and trachytes; 6—Upper Cretaceous limestones and marles (Campanian-Maastrichtian); 7—Upper Cretaceous dikes of rhyolites and dacites; 8—hypabyssal bodies of Upper Cretaceous rhyolites and dacites; 9—Upper Cretaceous volcanics (rhyolites, dacites, porphyrites) and pyroclastics (dacitic tuffs, agglomerates) with occasional interbeds of limestones and conglomerates (Turonian-Campanian); 10—small intrusions of Upper Cretaceous microdiorites; 11—sampling points; 12—K-Ar datings ((a) present work and (b) Dudauri et al. (1990)).

mass-spectrometer (SELMI) by the isotope dilution method with ^{38}Ar as spike (for more details, see Lebedev et al., 1999). The total blank of ^{40}Ar does not exceed 0.003 ng. The correction for atmospheric argon was made using isotope ratio $^{40}Ar/^{36}Ar = 295.5$. The values of constants recommended by IUGS were used for age calculations: $\lambda K = 0.581 \times 10^{-10}$ years^{-1}, $\lambda\beta = 4.962 \times 10^{-10}$ years^{-1}, and 40K = 0.01167 at.% (Steiger & Jäger, 1977). The results obtained yield close lying Campanian to Santonian ages: 78.7 ± 1.7 Ma (site BO15), 79.7 ± 1.6 Ma (site BO8), and 83.4 ± 1.8 Ma (site BO11) (uncertainties of reported K-Ar datings correspond to a 2σ level).

Besides these three K-Ar age determinations, additional age data are available for the study area. Dudauri et al. (1990) performed K-Ar age determinations on rhyodacites near the town of Korchulo, yielding ages of 74 ± 3 Ma, and 77 ± 3 Ma and on dacites from subvolcanic bodies near Bolnisi (57 ± 6 Ma), Kara-Torpak (56 ± 6 Ma), and Kvemo-Bolnisi (56 ± 8 Ma). Ages of sites without a specific radiometric date could be established by the type of volcanism and geographic position using a geological map from the Bolnisi area (Adamia et al., 1960) (Table 1 and Figure 1b).

3. Rock-Magnetic Experiments and Results

Rock-magnetic information can be useful for revealing the carriers of remanence, to gain knowledge about their magnetic properties, to assess their thermal stability and to preselect specimens for paleointensity experiments. Rock-magnetic investigations were conducted at the University of Burgos (Spain). Experiments with a variable field translation balance were carried out with the following measurement sequence: (i) isothermal remanent magnetization (IRM) acquisition curves up to 1 T, (ii) hysteresis curves, (iii) backfield

Table 1
Paleomagnetic Results

Site	Age	Lat (°N)	Lon (°E)	$N(n)$	$L + P$	DEC	INC	α_{95}	k	R	ΔR
BO1	uK	41.348	44.507	11	8 + 3	260.9	88.1	7.2	41.8	−89.7	171.6
BO2	uK, PG?	41.386	44.511	10	7 + 3	177.3	−62.8	6.2	64.1	6.7/2.7	11.1/10.9
BO3	PG	41.391	44.510	9(10)	9 + 0	349.9	62.6	6.0	74.3	−4.7	10.5
BO4	PG	41.398	44.516	11	11 + 0	19.3	54.2	6.0	59.2	−155.3	8.4
BO5	PG	41.401	44.515	10	10 + 0	339.2	48.2	5.1	89.8	−15.4	6.4
BO6	PG	41.403	44.525	12	10 + 2	345.6	56.8	7.1	39.0	−9.0	10.5
BO7	PG	41.413	44.523	10	2 + 8	19.2	29.4	6.5	64.1	180.0	6.3
BO8	79.7 ± 1.6	41.437	44.441	11	6 + 5	10.1	56.8	5.3	79.9	−160.5	8.1
BO9	PG	41.410	44.538	10	9 + 1	358.3	64.4	3.9	154.5	3.7	7.5
BO10	PG	41.453	44.525	11	11 + 0	38.3	56.3	3.4	176.8	−136.3	5.3
BO11	83.4 ± 1.8	41.455	44.564	10	10 + 0	128.2	32.1	6.2	60.8	−42.4	6.4
BO12	PG	41.457	44.535	9	9 + 0	39.3	56.9	2.2	541.1	−135.3	3.9
BO13	PG	41.456	44.534	13	9 + 0	41.3	56.8	5.1	103.8	−133.3	7.7
BO14(h)	uK	41.451	44.558	9	9 + 0	15.0	48.1	4.6	126.7	−155.6	6.1
BO14(m)				10	9 + 1	68.8	62.5	4.1	139.1	−101.8	7.5
BO15	78.7 ± 1.7	41.429	41.629	10(11)	10 + 0	84.8	56.0	3.5	195.3	−85.8	5.6
BO16	uK	41.429	44.627	10	10 + 0	82.6	41.0	2.5	371.3	−88.0	3.8
				Expected directions							
80 Ma				DEC = 350.6°; INC = 33.7°							
55 Ma				DEC = 354.6°; INC = 45.6°							

Note: Site: Flow number. In flow BO14, two paleomagnetic components were observed, BO14m and BO14h (see text). Age: Age of the flows: K-Ar data from the present study (in Myr) or Bolnisi area geological map data (Adamia et al., 1960); uK: upper Cretaceous; PG: Paleogene. Lat (°N) and Lon (°E): latitude and longitude data of sampled sites. $N(n)$: N is the number of samples used for flow mean calculation; in brackets, number of measured specimens; $(L + P)$: number of directly determined directions (L) and planes (P) used for calculation of flow mean. DEC and INC: Declination and inclination of ChRM. α_{95}: Radius of 95% confidence cone. k: Precision parameter. $R \pm \Delta R$: Rotation $R = D_0 - D_X$ where D_0 is the declination obtained in the present study and D_X is the expected one (uncertainties ΔR calculated after Demarest (1983)). The 80 Ma (55 Ma) expected direction is taken for upper Cretaceous (Paleogene) sites. In site BO2 both possible rotation values are calculated. 80 and 55 Ma: Expected upper Cretaceous (80 Ma) and Paleogene (55 Ma) directions calculated from the Apparent Polar Wander Path (APWP) for Europe (Besse & Courtillot, 2002).

curves (iv), and strong-field (38 mT) magnetization vs. temperature (M_S-T) curves measured in air. All these experiments were performed on powdered specimens selected from all studied flows. Furthermore, susceptibility vs. temperature (k-T) curves were measured with a Kappabridge KLY-4 device connected to a CS3 furnace in an applied field $H_{app} = 300$ A/m on some powdered specimens. This experiment was carried out in an argon atmosphere, heating, and cooling down samples between room temperature and 700 °C at a rate of 15 °C/min.

Before starting to record thermomagnetic M_S-T curves, a 1-T field was applied to the samples, so that they acquired a (near) saturation magnetization. Subsequently, samples were heated up to 600 or 700 °C and cooled down to room temperature in air at a rate of 20 or 30 °C/min. In addition, a succession of heating-cooling cycles from room temperature to 350, 450, and 580 °C was performed on seven selected samples. Data analysis was carried out with the RockMagAnalyzer 1.0 software (Leonhardt, 2006). After correction for the diamagnetic and paramagnetic contribution, hysteresis parameters were obtained from hysteresis and backfield curves. Determination of Curie temperatures (T_C) in M_S-T curves was performed both with the two-tangent method (Grommé et al., 1969) and the second derivative technique included in the RockMagAnalyzer 1.0 software, yielding qualitatively (and generally, quantitatively) similar results. k-T curves

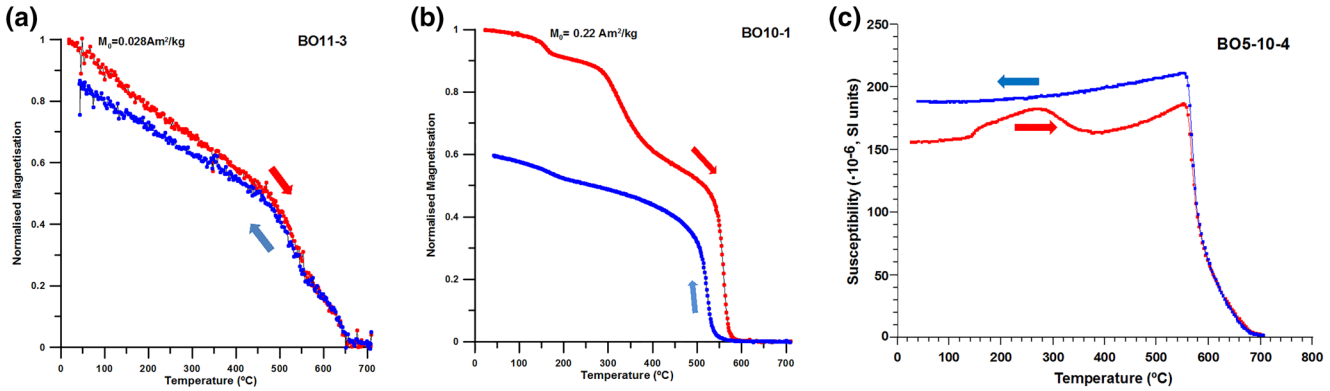

Figure 2. Thermomagnetic curves. Magnetization vs. temperature curves of (a) sample BO11-2 (type H) and (b) sample BO10-3-3. (c) Susceptibility vs. temperature curve of sample BO5-10-4. Heating curves in red, cooling curves in blue.

were measured on eight selected samples and inflexion points after the susceptibility drop following Hopkinson peaks were taken to determine Curie temperatures.

Only specimens from three flows (BO8, BO11, and BO14) displayed reversible M_S-T curves (type H curves, Figure 2a), showing either one or two ferromagnetic (s.l.) phases. In all cases, a phase with T_C between around 660 and 680 °C (both in the heating and cooling curves) was observed, which can be ascribed to hematite, especially if results from IRM acquisition curves and hysteresis loops (see below) are taken into account. In addition, in flows BO8, BO11 a second phase showing a T_C around 560 °C related to low-Ti titanomagnetite could be recognized. In site BO5, an apparently reversible M_S-T curve was also obtained, which showed a single ferromagnetic (s.l.) phase with a T_C around 585 °C both in the heating and cooling branch, which can be ascribed to magnetite. However, in this case, the thermomagnetic curve was not recorded continuously up to a peak temperature of 700 °C, but it consisted of a succession of three heating-cooling cycles from room temperature to 350, 450 and 580 °C. In a k-T curve recorded on the same sample between room temperature and 700 °C, besides magnetite another phase (T_C = 330 °C) could be recognized on the heating, but not on the cooling branch (Figure 2c).

The remaining studied samples were characterized by a rather complex behavior and irreversible M_S-T curves (type-M curves, Figure 2b). The heating branch of the curves showed between two and four ferromagnetic (s.l.) phases. In all type-M curves, a phase with high Curie temperatures between around 555 and 585 °C was observed, which can be related to low-Ti titanomagnetite (or slightly Mg-substituted or Al-substituted magnetite). Moreover, another phase with intermediate T_C, in most cases ranging between around 300 and 450 °C could also be recognized. In most type-M samples, this is the strongest observed ferromagnetic (s.l.) phase, which can be probably related to titanomaghemite. Additionally, in a few samples, a low Curie-temperature phase (T_C < 200 °C) was observed. Finally, two specimens also displayed an unstable high Curie-temperature phase (observed apparent T_C around 640 °C), possibly maghemite. The cooling curve of type-M samples showed much lower magnetization values than the heating curve and only a main phase, with a near-magnetite T_C, although a very weak contribution of a phase with the Curie temperature of hematite could also be detected. T_C of the near-magnetite phase was in all cases slightly lower than in the heating curves, which may be ascribed to cation reordering during heating (Bowles et al., 2013). To find out at which temperatures alteration started in type-M samples, some specimens were subjected to thermomagnetic experiments with increasing maximum heating temperatures, and moderate alteration could be recognized after heating to 350 or 450 °C.

IRM acquisition curves show in most cases rapid saturation, and at an applied field of 200/300 mT more than 90% of the SIRM is already acquired (Figure S1a). In such cases, remanence can be related to low-coercivity ferrimagnetic phases, although in other cases also a minor high-coercivity phase could be observed. In some cases, however, samples which cannot be saturated with applied fields of 1 T were observed (Figure S1b). This behavior is ascribed to the presence of hematite.

Hysteresis curves with spreading middles and slouching shoulders (so-called potbellies) were mainly found (Figure 3a) among the Bolnisi samples, as shown by mostly negative values of the shape parameter σ

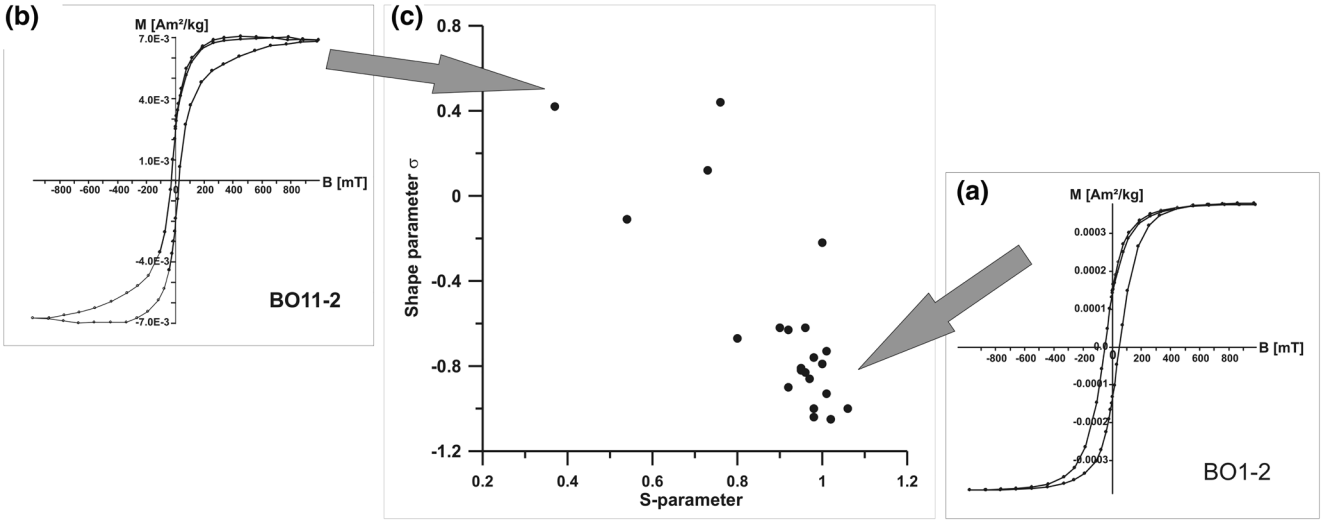

Figure 3. Hysteresis curve results. (a) Potbelly shaped hysteresis curve of sample BO11-2; (b) wasp-waisted shaped hysteresis curve of sample BO1-2; (c) relation of shape parameter σ (Fabian, 2003) and S-parameter (Bloemendal et al., 1992).

(Fabian, 2003). Nevertheless, in two cases, hysteresis curves with constricted middles (so-called wasp-waisted loops) were observed (Figure 3b) while in a few other cases shape parameters did not differ much from 0, the latter pointing to a simpler hysteresis behavior. Distorted hysteresis loops can be produced by mixtures of different magnetic phases and/or domain states (e.g., Pick & Tauxe, 1994; Tauxe et al., 1996). Thermomagnetic and IRM acquisition curves have already shown that the magnetic mineralogy of the Bolnisi samples is rather complex, with different phases with clearly different coercivities being observed. Figure 3c shows the relation of shape parameter σ with the S-parameter (Bloemendal et al., 1992), indicating that samples with hysteresis curves of more pronounced potbelly characteristics appear related to a lower presence of high-coercivity minerals. On a Day-diagram (Day et al., 1977; Figure S2), some samples plot near the superparamagnetic (SP) saturation envelope (Dunlop, 2002). However, no clear relation appears between higher negative shape parameter σ values (more potbelly like behavior) and SP grain content. It should be borne in mind that information provided by Day diagrams is often ambiguous, as hysteresis parameter ratios may be influenced by various conditions (Roberts et al., 2018).

4. Paleomagnetic Measurements and Results

All paleomagnetic measurements were carried out at the paleomagnetic laboratory of the University of Burgos (Spain). Remanence was measured with a superconducting 2G cryogenic magnetometer. From each site, three or four pilot specimens were chosen and subjected to either alternating field (AF) or thermal demagnetization, so that both methods were tested for all sites. Subsequently, the most suitable demagnetization technique for each case was selected. Thermal demagnetization was performed with a TD48-DC (ASC) furnace and AF-demagnetization with a degausser included in the 2G magnetometer system. Analysis of demagnetization data was carried out with the Remasoft software (Chadima & Hrouda, 2006) and to calculate directions of remanence components, principal component analysis (Kirschvink, 1980) was used.

Natural remanent magnetization (NRM) mean site directions which apparently display normal polarity are observed in all sites. However, in several cases, a large scatter as well as rather anomalous directions with declinations largely deviating from North can be recognized. The observed high α_{95} values suggest the presence of viscous or secondary components in several lavas. Analysis of NRM demagnetization shows that seven flows basically display a main paleomagnetic component and a minor viscous component (Figure 4a) while the remaining nine flows are characterized by the presence of two paleomagnetic components, which sometimes overlap (Figure 4b). However, in some cases, in these latter nine flows single-component specimens are also observed.

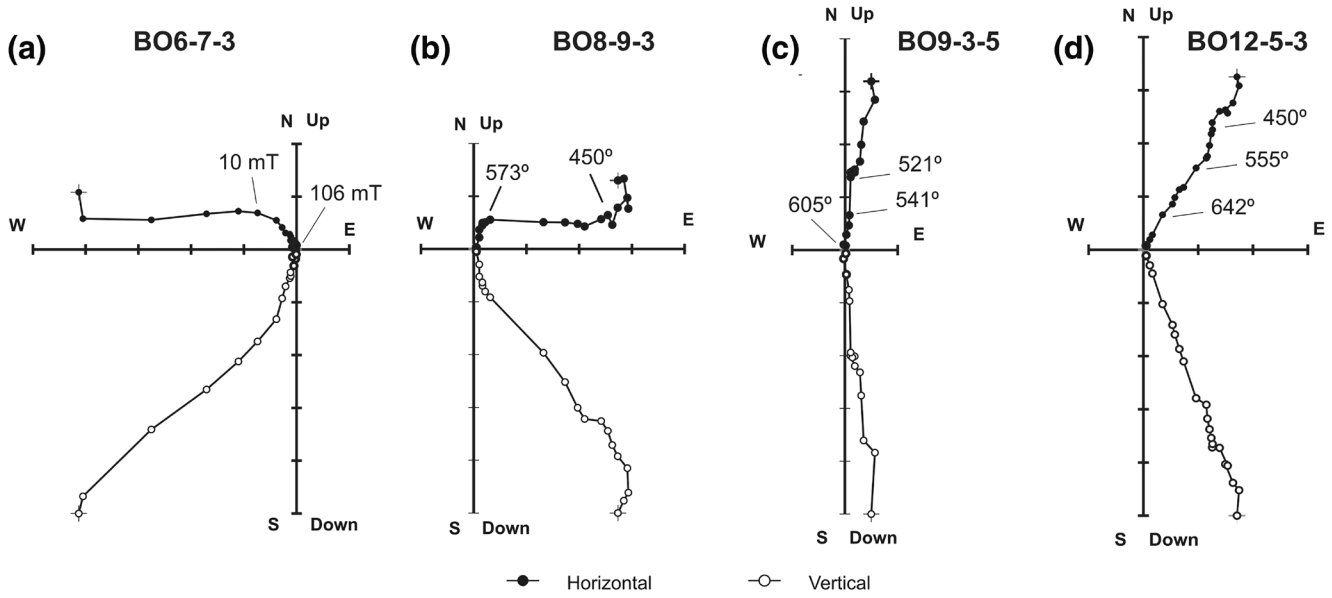

Figure 4. Orthogonal demagnetization vector plots. (a) AF-demagnetization of sample BO6-7-3; (b) thermal demagnetization of sample BO8-9-3; (c) thermal demagnetization of sample BO9-3-5; (d) thermal demagnetization of sample BO12-5-3. Horizontal projection: closed symbols; vertical projection: open symbols.

As shown in Table 1, normal-polarity characteristic remanence (ChRM) directions were determined in all cases except in site BO2, which produced a reverse-polarity mean direction. In flow BO14, two different normal-polarity ChRM components were distinguished, one associated to the presence of hematite and another to magnetite. Nearly 90% of the directly determined directions were associated to MAD values ≤5.0°, with an average MAD value of 2.8°. For the interpretation of demagnetization diagrams involving two overlapping components, analysis of remagnetization circles had to be employed and in some samples belonging to seven flows, paleodirections could not be directly determined and only remagnetization circles were obtained. Therefore, in these flows mean paleomagnetic directions had to be calculated combining remagnetization circles and directly determined directions (McFadden & McElhinny, 1988).

5. Paleointensity Experiments

5.1. Thellier-Type Paleointensity Determinations with the IZZI Protocol

Paleointensity determinations have been carried out at the paleomagnetic laboratory of the University of Burgos with the IZZI method (Yu et al., 2004), which can be helpful to detect the presence of so-called pTRM tails. Sample preselection for the IZZI method paleointensity experiments was mainly based on the results obtained on paleomagnetic experiments, and only specimens displaying a basically univectorial character without a strong viscous component were chosen for the experiments. Rock-magnetic results were only taken for a cruder distinction of magnetic characteristics. While only few flows met the conditions to be considered suitable for paleointensity determinations, specific samples from some other flows apparently displayed adequate conditions for preselection, so that they also were included in the paleointensity experiments.

Small irregular fragments from 65 specimens belonging to nine different flows were broken from standard samples and fixed in boron-silicate vials of 10-mm diameter, which were marked to keep the orientation. IZZI experiments were performed in a TD-48 (ASC) oven in argon atmosphere to avoid or at least reduce oxidation. The experiment consisted of a sequence of 11 double steps at increasing temperatures between room temperature and 620 °C, using a laboratory field B_{lab} = 40 μT, which was applied along the axis of the oven, so that the specimens' magnetization was oriented at random with respect to the applied field. Before cooling, samples were left about 15 min at the peak temperature at each heating step. Subsequently, samples were left cooling by themselves for several hours. During the experiment, up to six pTRM checks were performed at different temperatures.

Sánchez-Moreno et al. (2020) analyzed a basaltic lava flow sequence in Georgia with different Thellier-type experiments, leaving in one experiment samples cooling naturally and in the other experiment with a fan. Although the difference in cooling time between both cases is one order of magnitude, no differences were observed in the results. Volcanic units in the present study are somewhat thicker than those analyzed by Sánchez-Moreno et al. (2020), so that cooling time has been estimated to be moderately longer. Our experimental approach leaving samples cool down naturally intends to reduce cooling rate effects.

No banded features have been observed in the studied volcanic units neither at a macroscopic nor microscopic level and we have not considered necessary to perform an anisotropy of thermoremanence analysis to account for anisotropy effects on paleointensity determination.

Analysis of paleointensity results was performed with the Thellier-Tool (version 4.22) software (Leonhardt et al., 2004), using criteria included in this software to select successful determinations. Furthermore, to evaluate the existence of remanent magnetization carried by MD grains, the shape of Arai plots was assessed visually, excluding from further interpretation those clearly showing a concave shape. Two quality levels of different strictness (C1 and C2) were chosen as selection criteria thresholds and are listed in Table 2. The chosen thresholds are basically those proposed by Paterson et al. (2014) for the modified Thellier-Tool A and B criteria sets (Leonhardt et al., 2004), except for fraction factor f for C1 determinations, which is kept at 0.5 as in the original criteria set. Application of these criteria to our results yielded only 17 successful determinations (2 class C1 and 15 class C2) out of 65 (26.1%), mainly belonging to flows BO8 and BO9 (Figure 5). The remaining unsuccessful paleointensity determinations were rejected because of alteration detected by pTRM checks, concave-shaped Arai diagrams pointing toward remanence carried by MD grains (Figure 5b) and unsuitable samples due to two overlapping components.

In flows BO9 and BO15, in most cases, Arai diagrams showed steps at the lowermost temperatures (150 °C and a few subsequent steps) that deviate from the linear trend drawn by the steps above 350 °C (Figures 5b and Figures 5c). Although no strong disagreement is observed in these samples between directions at lower and higher demagnetization temperatures, several specimens display moderate directional discrepancies which might be ascribed to a viscous overprint. In all specimens from both sites in which paleointensity determinations fulfill reliability criteria, only steps above 350 °C (BO9) or 400 °C (BO15) have been taken into account (Table 2). In site BO9, six specimens fulfill reliability criteria and one of them belongs to class C1 determinations. All yield rather similar results, so that a reliable mean paleointensity is obtained. Only two paleointensity determinations fulfilling reliability criteria were obtained for site BO15, although one of them also belongs to class C1. Results are very similar to those from BO9.

At the site level, the threshold required for scatter was standard deviation $\sigma_{SITE} \leq 15\%$ or $\sigma_{SITE} \leq 5$ μT. As shown in Table 2, only mean results obtained in flows BO8 and BO9 are based on >3 determinations, but mean paleointensities of flows BO12 and BO15, which are based on only two successful paleointensity determinations, show low standard deviations at the site level (<5 μT). All four of these flows yield mean paleointensity values around 20 μT, less than half the current field strength of nearly 50 μT at the same site.

5.2. Multispecimen Paleointensity Determinations

Additional paleointensity determinations were carried out with the multispecimen method (Dekkers & Böhnel, 2006) at the paleomagnetic laboratory of UNAM in Morelia (Mexico). These experiments included the protocols for fraction (FC) and domain-state correction (DSC) put forward by Fabian and Leonhardt (2010). Fourteen standard paleomagnetic samples from seven sites were divided into eight subspecimens and pressed into salt pellets with the size and shape of standard paleomagnetic specimens (112 in total). The multispecimen method was carried out at three different temperatures (350, 480, and 550 °C), based on the Curie temperatures estimated from M_S-T curves for each flow. Experiments were performed with an ASC Scientific TD48-SC oven, applying fields between 10 and 60 μT with increments of 10 μT. For each heating step, the specimens were kept for 20 min at the selected temperature. Cooling was fan assisted (about 40 min to cool down from ~500 °C to room temperature). The following experimental sequence was applied with remanence being measured with an AGICO JR6 spinner magnetometer: (i) measurement of NRM; (ii) orientation of subspecimens with their NRM directions parallel to the axis of the heating

Table 2
Palaeointensity Results

IZZI paleointensity determinations											
Selection criteria		N	F	q	σ/slope	d(CK)		MAD (°)	α (°)		
Thresholds C1		≥5	≥0.5	≥5	≤0.1	≤7		≤6	≤15		
Thresholds C2		≥5	≥0.35	≥1	≤0.15	≤9		≤15	≤15		
Threshold site level		$\sigma_{SITE} \leq 15\%$ or $\sigma_{SITE} \leq 5$ μT									
Sample	Range	N	f	Q	σ/slope	d(CK)	MAD (°)	α (°)	F (μT)	ΔF (μT)	Class
BO8-1-3	20–560	10	0.642	6.0	0.0872	2.4	3.3	1.7	21.6	1.9	C1
BO8-2-4	20–580	11	0.90	8.6	0.086	2.1	5.7	6.0	16.0	1.4	C1
BO8-3-2	250–560	8	0.58	4.4	0.099	2.8	2.4	3.4	27.7	2.7	C2
BO8-4-2	400–560	6	0.39	1.9	0.148	2.1	2.3	4.3	21.2	3.1	C2
BO8						21.6 ± 4.8 μT					
BO8 + MS						22.5 ± 4.6 μT					
B09-2-2	350–580	8	0.53	2.5	0.148	6.1	5.9	10.8	16.8	2.5	C2
BO9-4-4	350–580	8	0.54	3.6	0.113	8.9	2.6	5.4	18.4	2.1	C2
BO9-5-4	350–620	9	0.75	5.8	0.108	5.7	8.9	9.1	21.7	2.4	C2
BO9-6-4	350–580	8	0.61	3.6	0.129	5.9	7.5	13.9	14.9	1.9	C2
BO9-7-4	350–620	9	0.67	6.0	0.087	3.4	4.2	3.4	21.2	1.8	C1
BO9-8-5	350–620	9	0.69	6.5	0.086	4.9	7.9	9.3	17.3	1.5	C2
BO9						18.4 ± 2.6 μT					
BO12-5-4	250–620	10	0.54	4.0	0.112	8.8	4.8	9.9	23.8	2.6	C2
BO12-7-2	350–620	9	0.52	6.3	0.065	7.0	2.5	0.4	22.2	1.5	C2
BO12						23.0 ± 1.1 μT					
BO15-5-3	400–580	7	0.357	1.5	0.107	4.5	2.4	4.6	14.2	1.5	C2
BO15-9-3	400–620	8	0.65	7.4	0.071	4.9	3.5	4.9	20.3	1.5	C1
BO15						17.3 ± 4.3 μT					
BO10-7-3	350–580	8	0.510	3.0	0.096	8.7	3.8	4.4	7.8	0.7	C2

Multispecimen paleointensity determinations							
Selection criteria		R^2		ε_{alt}		Δb/Int	
Thresholds		≥0.9		≤15		$\lvert\Delta b\rvert \leq 0.15$ and/or within error	
		DB	FC	DSC	DB,corr	FC,corr	DSC,corr
BO8-2-4	N	5	4	4	5	4	4
	F	25.9	26.2	22.1	25.8	26.1	22.2
	$F_{Min} - F_{Max}$	21.5–31.0	22.9–33.6	26.4	31.1	33.2	26.6
	ε_{alt}	−5.0	−6.2	−6.2	−4.8	−6.0	−6.0
	R^2	0.884	0.952	0.980	0.877	0.952	0.987
	Δb/Int	—	−0.46/Yes	−0.53/No	—	−0.45/Yes	−0.52/No
BO16-2-4	N	3	3	3	3	3	3
	F	67.8	73.8	55.7	67.7	73.7	55.6
	$F_{Min} - F_{Max}$	67.4–76.8	73.3–75.3	55.2–56.1	67.3–76.6	73.1–75.3	55.1–56.1
	ε_{alt}	−14.8	−14.8	−14.8	−14.6	−14.6	−14.6
	R^2	0.869	0.998	1.000	0.868	0.997	1.000
	Δb/Int	—	−0.15/NO	−0.24/NO	—	−0.15/NO	−0.24/NO

Table 2
Continued

Mean Bolnisi results		
	Paleointensity (μT)	VADM (Am^2)
Upper Cretaceous sites BO8 and BO15	19.9 ± 3.7 μT	3.4×10^{22}
Paleogene sites BO9 and BO12		

Note: ZZI determinations: Selection criteria and threshold values for class C1 and C2. *N*: Number of NRM-pTRM points used for paleointensity determination. *f*: Fraction of extrapolated NRM used; *f* is referred to the so-called "true NRM," which is the intersection between linear fit and *y* axis (Leonhardt et al., 2004). σ/slope: Ratio of the standard error of the slope and the slope of the NRM-TRM diagram. *q*: Quality factor (Coe et al., 1978). *d*(CK): Difference between the pTRM check and original TRM value at a given temperature normalized to the TRM (Leonhardt et al., 2000). MAD: Mean angular deviation of NRM end-point directions at each step obtained from palaeointensity experiments. α: Angle between the vector average of the data selected for palaeointensity determination and the principal component of the data. σ_{SITE}: Standard deviation of the site mean. IZZI results: Sample: Sample name; range: Temperature interval in °C used for paleointensity determination. $F \pm \Delta F$: Paleointensity estimate for a single specimen and its standard error; standard error of the paleointensity estimate is calculated by the product of the standard error of the best-fit line in the Arai plot and the laboratory field. Class: Quality level of paleointensity determination. Mean flow paleointensity values and their standard deviation are shown for those flows with at least two successful paleointensity determinations. BO8 + MS: Mean paleointensity obtained from five IZZI and one multispecimen determination in site BO8 (see text). Multispecimen determinations: ε_{Alt}: Average alteration parameter. R^2: Quality of the linear least-squares fit. Δ*b*/Int: Check of whether the linear fit intersects the ordinate axis through (0.-1) within 15% ($\Delta b \leq 0.15$) and/or within error (Yes or No). Multispecimen results: DB, FC, and DSC: standard, fraction, corrected and domain-state corrected determination. DB,corr, FC,corr, and DSC,corr: Alignment-corrected standard, fraction-corrected determination, and domain-state corrected determination. *n*: Number of specimens used for paleointensity determination. *F*: Paleointensity result. $F_{Min} - F_{Max}$: Paleointensity determination uncertainty bounds. Mean Bolnisi results: Mean paleointensity results and VADM of the Bolnisi sites (see text), weighted and unweighted (in brackets). Mean results obtained from upper Cretaceous sites BO8 and BO15 and Paleogene sites BO9 and BO12 are shown.

chamber and subsequent heating in an axial field; (iii) specimens as in the previous step but with an inverted laboratory field direction; (iv) specimens reheated in zero field; and (v) repetition of step (ii).

All calculations (relative differences between pTRMs and NRMs) were performed with the VBA software developed by Monster et al. (2015b). Parameter α (Fabian & Leonhardt, 2010) was set to $\alpha = 0.5$ for the calculations. The quality of the linear least-squares fit (R^2), the relative alteration error value (ε_{alt}, Fabian & Leonhardt , 2010) and the check of whether the linear fit intersects the ordinate axis through (0.-1) within 15% and/or within error, have been taken as selection criteria for reliable determinations. Threshold values are listed in Table 2. Monster et al. (2015a and 2015b) proposed for the relative alteration error value ε_{alt} a probably too strict threshold of $\varepsilon_{alt} = 3\%$. Here, we use the threshold $\varepsilon_{alt} < 15\%$ proposed by Sánchez-Moreno et al. (2018b). Several samples did not provide meaningful results, mostly linked to the presence of two paleomagnetic components. Among the samples apparently displaying significant results, only two (BO8-2-4 and BO16-2-4, Table 2 and Figure 5c) fulfilled the proposed criteria, and in both cases only the fraction corrected (without and with alignment correction) value. In several other cases, samples are affected by alteration or the linear fit fails to pass the ordinate axis through (0.-1) within the proposed threshold.

6. Discussion

6.1. Paleomagnetic Directions

In Figure 6, mean directions obtained in each flow (two in the case of BO14) are shown together with expected upper Cretaceous to Paleogene directions calculated from the European Apparent Polar Wander Path (APWP) for three different ages (55, 70, and 80 Ma) as determined by Besse and Courtillot (2002) using 10 Myr windows. As can be easily recognized in Figure 6 and Table 1, results do not agree with the expected values. As the studied samples stem from volcanic units and no sedimentary strata of suitable age were available to obtain information about possible dips the sampled units might have experienced, paleomagnetic values are not bedding-corrected and include the sum of all possible movements experienced by the volcanic units since their eruption. Table 1 and Figure S3 show the rotation $R = D_0 - D_X$ and flattening $F = I_X - I_0$ values, where D_0 and I_0 are, respectively, the declination and inclination values obtained in the present study and D_X and I_X the expected ones. As can be recognized, flattening *F* values are low, as measured inclination values are only moderately higher than expected ones. The only exception is site BO1, which yields an anomalous nearly vertical inclination. On the other hand, while declination values of several sites correspond to nearly North-South directions, several other sites show eastward deviated

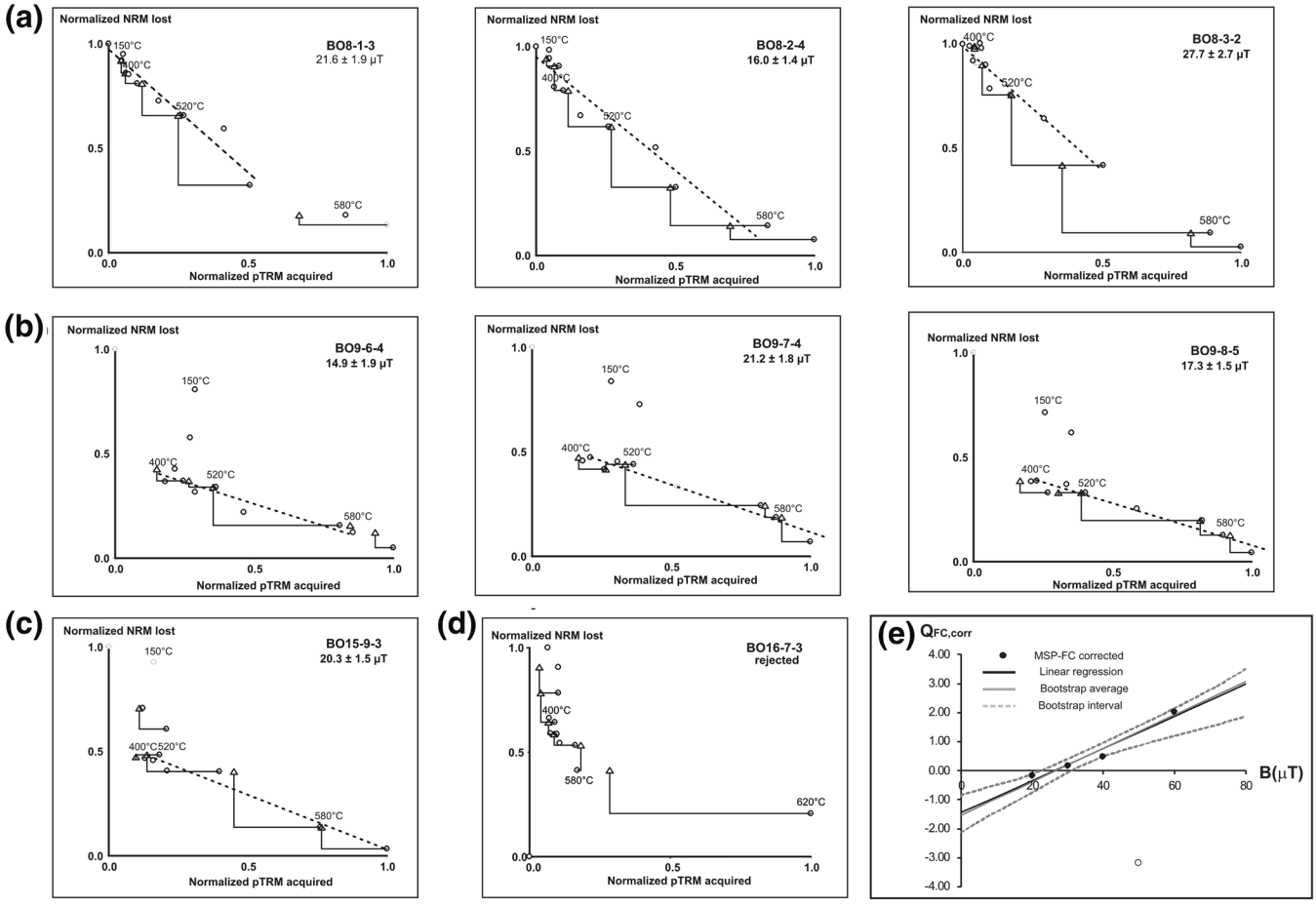

Figure 5. Paleointensity determinations. IZZI paleointensity determinations: (a) flow BO8 (samples BO8-1-3; BO8-2-4; BO8-3-2); (b) flow BO9 (samples BO9-6-4; BO9-7-4; BO9-8-5); (c) flow BO15 (sample BO15-9-3); (d) Failed IZZI paleointensity determination on sample 16-7-3; (e) Multispecimen paleointensity (MS) determination (fraction and alignment corrected) on sample BO8-2-4. Closed (open) dots represent used (rejected) MS data.

paleodeclinations, especially in BO11, BO15, and BO16. Only site BO1 shows a clearly different declination which is, however, affected by a particularly high uncertainty due to its very steep inclination.

In view of the observed features of paleomagnetic directions, the studied units seem to have been mainly affected by (nearly) vertical-axis rotations but to a different extent in different sites. The fact that only declinations but not inclinations show larger discrepancies with the expected values seems to discard anomalous EMF features as the origin of the observed paleomagnetic results, except perhaps for site BO1. As can be recognized in Figure 7, paleodeclinations display a different behavior in different zones of the relatively small study area. The sites in its southern part (BO2, BO3, BO4, BO5, BO6, BO7, BO8, and BO9), which has been tagged zone A in the map, display an unrotated northerly declination ($D = 1.1° \pm 14.2°$), while the sites in the northern sector (zone B, sites BO10, BO11, BO12, BO13, BO14, BO15, and BO16) display a strongly clockwise rotated paleodeclination ($D = 72.9° \pm 26.6°$).

It can be recognized in Figure 7 that all sites included in zone A, which seem to have not experienced significant vertical-axis rotations, lie in the two nearly NNE-SSW oriented Poladauri and Mashavera river valleys (Figure 1), possibly related to the NW-SE fault system mentioned above. Its strike has a similar direction than the nearly N-S compression due to the convergence of the Eurasian and African-Arabian plates since

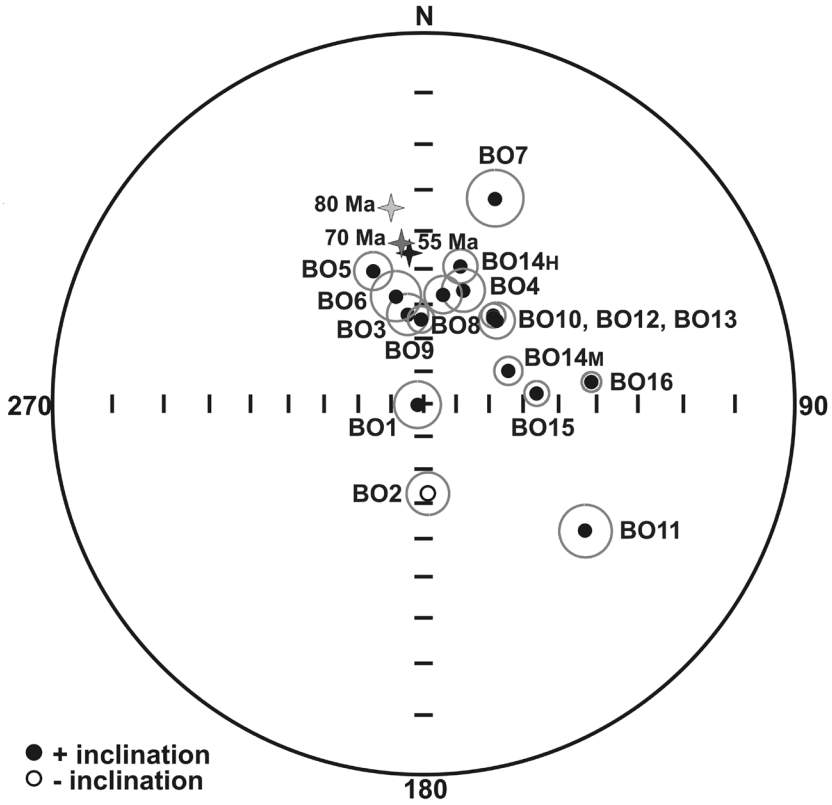

Figure 6. Paleomagnetic results. Stereographic projection of mean paleomagnetic directions obtained in each site (two directions are shown for site BO14, see text) with α_{95} confidence cones. Solid (open) circles are for normal (reversed) polarities. Expected upper Cretaceous and Paleogene directions for 80, 70, and 55 Ma, calculated from the Apparent Polar Wander Path (APWP) for Europe (Besse & Courtillot, 2002) are also shown.

the start of continental collision and than present-day velocities of the study region relative to Eurasia obtained from GPS data (Reilinger et al., 2006). On the other hand, zone B sites lie near the nearly E-W oriented Mashavera river valley. Thus, paleomagnetic results suggest that as a result of the stress produced by the continental collision since Oligocene in the Bolnisi area, deformation has been accommodated in different

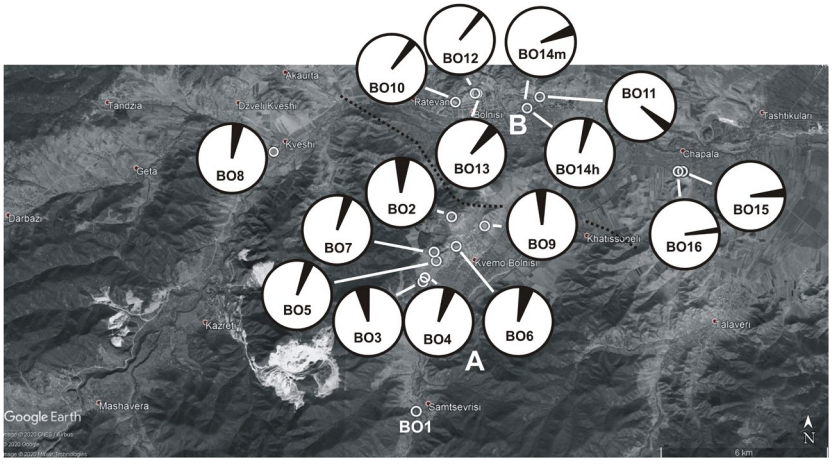

Figure 7. Paleomagnetic rotations. Paleomagnetic declinations with confidence limits (Demarest, 1983) obtained in the Bolnisi area. Adapted from Google Earth.

ways on a relatively small scale depending on the orientation of faults enclosing the studied sites, with some sites experiencing strong clockwise vertical-axis block-rotations and others no rotations at all.

6.2. Paleointensity Results

Paleointensity determinations with the IZZI method yielded 15 (4 class 1 and 11 class 2) successful determinations out of 65. Most successful determinations stem from site BO9 (6) and BO8 (4). Results from flows BO15 and BO12 are based on only two successful determinations while another flow (BO10) only produced one successful determination. All flow mean paleointensities based on at least two determinations yield very similar results around 20 μT. Only two successful paleointensity determinations fulfilling all proposed criteria and thresholds could be obtained with the multispecimen method. Sample BO8-2-4 yielded a (fraction and alignment corrected) paleointensity $F_{FC,corr} = 26.1$ μT, similar to the results obtained with the IZZI method, while sample BO16-2-4 yielded a high (fraction and alignment corrected) paleointensity $F_{FC,corr} = 73.7$ μT. No successful determinations were obtained in that flow with the IZZI method.

The agreement of results obtained with both different kinds of paleointensity determination methods will be taken as a strong reliability criterium for successful determinations, as the coincidence of the result of two wrong determinations would be highly unlikely. We will consider that two paleointensity determinations yield the same result if the difference between them is <8 μT, because the use of relative differences could imply too small uncertainties for experimental results in the case of weak paleointensities. The 8 μT value has been chosen taking 15% of the current field in Georgia, as suggested by Sánchez-Moreno et al. (2018b).

The joint analysis of Thellier-type and multispecimen results led us to distinguish the following possibilities and determination quality classes:

Class 1. Successful IZZI paleointensity mean site results (three or more successful determinations) agree with a successful multispecimen determination in the same site

Class 2.

(a) IZZI paleointensity mean site results based on less than three successful determinations agree with a successful multispecimen determination in the same site or
(b) Successful IZZI paleointensity mean site results (three or more successful determinations) are available but do not agree with a successful multispecimen determination in the same site or no multispecimen result is available

Class 3.

(a) An IZZI paleointensity mean site result is based on two agreeing successful determinations but does not match a successful multispecimen determination in the same site or no multispecimen result is available

Class 4.

(a) A single successful IZZI result is available, which does not agree with a successful multispecimen determination in the same site or no multispecimen result is available
(b) A successful multispecimen result is available but no IZZI results

Successful IZZI determinations are available from flows from six sites and successful multispecimen determinations in two flows. Only site BO8 yields a class 1 result, as the mean result obtained from four successful IZZI determinations agrees with the multispecimen result. The final mean value has been calculated giving the multispecimen result the weight of a single sample, as it has been obtained from an experiment based on a single sample. Thus, the result from BO8 is based on five determinations and is especially supported by the matching results from two different methods. Site BO9 yields a class 2 result, based on six successful Thellier-type determinations. Results from sites BO12 and BO15 are based on two successful IZZI determinations, but no multispecimen results are available, and they are ascribed to class 3. Finally, the results obtained in site BO10 belongs to class 4.

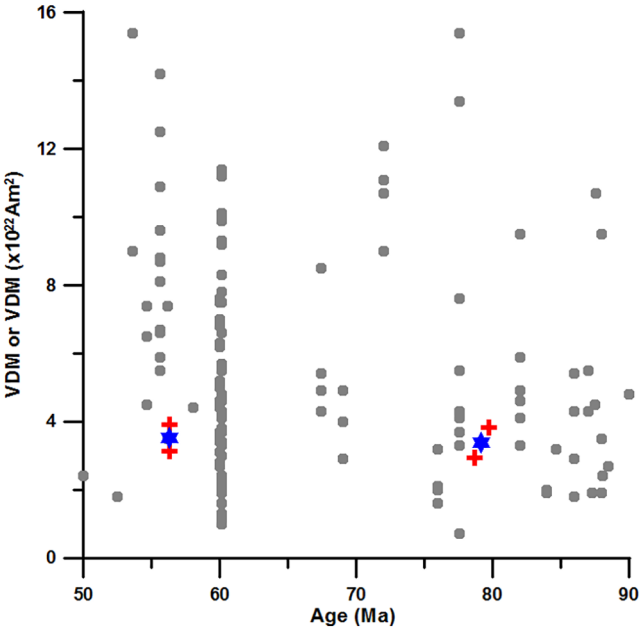

Figure 8. Late Cretaceous and Paleogene V(A)DMs. Paleogene and Late Cretaceous virtual (axial) dipole moments from the PINT and MagIC databases (Biggin et al., 2010; Tauxe et al., 2013) and the World Paleointensity Database from the Borok Geophysical Observatory (http://wwwbrk.adm.yar.ru/palmag/database_e.html) obtained from Thellier-type experiments with pTRM checks including microwave experiments in the 50–90 Ma age interval. Upper Cretaceous and Paleogene results obtained in the present study at a flow level are shown with red crosses and mean Cretaceous and Paleogene values with blue stars. All used references are listed in Table S2 (Supporting Information).

The result from class 4 was not taken into account for any further consideration, as it is only based on a single piece of information not confirmed by a second result. Among the flows yielding valid results, site-specific K-Ar ages are only available for flows BO8 and BO15, which are of upper Cretaceous age. Sites BO9 and BO12, on the other hand, are of Paleogene age (Table 1). A mean paleointensity value $F_{uK} = (19.9 \pm 3.7)$ μT is thus obtained for the upper Cretaceous sites and a mean paleointensity value $F_{Pg} = (20.7 \pm 3.3)$ μT for the Paleogene flows. Mean paleointensity results and virtual axial dipole moments (VADM) calculated using the geographic colatitude of the sites is listed in Table 2.

Figure 8 shows Paleogene and Late Cretaceous (50–90 Ma age interval) virtual (axial) dipole moments obtained from Thellier-type experiments with pTRM checks (including microwave experiments), obtained from samples of normal or reversed polarity. Data were selected from the PINT and MagIC databases (Biggin et al., 2010; Tauxe et al., 2013) and the World Paleointensity Database from the Borok Geophysical Observatory (http://wwwbrk.adm.yar.ru/palmag/database_e.html). Although 10 out of the 55 Late Cretaceous records display dipole moments with values higher than the current dipole moment of $\sim 8 \times 10^{22}$ Am^2, most V(A)DMs are rather low, generally below 5×10^{22} Am^2, like the Late Cretaceous VADM $= 3.4 \times 10^{22}$ Am^2 obtained in the present study. Also, in the 50–65-Ma interval, V(A)DMs from the PINT database show dipole moments predominantly lower than the present-day one (64 of 81 entries), and approximately half of them lie below 5×10^{22} Am^2. The highest dipole moments were obtained on single plagioclase crystals from lavas from the Emperor seamounts (Tarduno & Cottrell, 2005) and from basalts from West Greenland (Riisager & Abrahamsen, 2000; Riisager et al., 1999). Our Paleogene low VADM from the Bolnisi data (3.5×10^{22} Am^2) agrees with the general trend of lower dipole moments.

Paleointensity results from several studies from the last 2 decades suggest that the average dipole moment during stable polarity periods of the EMF is clearly lower than its present value (e.g., Juárez et al., 1998; Selkin & Tauxe, 2000; Tauxe, 2006). The Late Cretaceous and Paleogene VADMs obtained in the present study support this conclusion.

7. Conclusions

A paleomagnetic and paleointensity study including new K-Ar determinations has been carried out on a suite of 16 rhyolitic and dacitic lavas of Cretaceous and Paleogene age.

K-Ar determinations performed on three sites yield close lying Campanian to Santonian ages: 78.7 ± 1.7, 79.7 ± 1.6, and 83.4 ± 1.8 Ma.

Paleointensity determinations were performed with the IZZI method on 65 specimens from nine different flows, yielding only 15 successful determinations on samples belonging to five flows (success rate 23.1%). In addition, 14 samples from seven sites were subjected to the multispecimen paleointensity determination method, but only two samples fulfilled all selection criteria. The joint analysis of Thellier-type and multispecimen results yielded a paleointensity result $F_{uK} = (19.9 \pm 3.7)$ μT for the upper Cretaceous sites. Furthermore, a mean paleointensity $F_{Pg} = (20.7 \pm 3.3)$ μT was obtained for the Paleogene flows. VADMs obtained for the Late Cretaceous (3.4×10^{22} Am^2) and Paleogene (3.5×10^{22} Am^2) agree with the main trend observed in other studies and support the idea of a lower average dipole moment during stable polarity periods as suggested by different sources (e.g., Juárez et al., 1998; Selkin & Tauxe, 2000; Tauxe 2006).

Mean flow directions obtained in paleomagnetic experiments do not agree with expected upper Cretaceous to Paleogene directions calculated from the European APWP. Inclination results roughly agree with expected values, but while declination values of several sites correspond to nearly North-South directions ($D = 1.1° \pm 14.2°$), several other ones show clearly eastward deviated paleodeclinations ($D = 72.9° \pm 26.6°$). These paleomagnetic results suggest that nearly vertical-axis rotations have taken place in the study area, possibly due to the stress generated by the continental collision since Oligocene. Deformation has been accommodated in different ways on a relatively small scale depending on the orientation of faults enclosing the studied sites, with some sites experiencing strong clockwise vertical-axis block-rotations and others no rotations at all.

Data Availability Statement

Data sets for this research are available under the following reference: Calvo-Rathert et al. (2020), http://doi.org/10.5281/zenodo.3997235

Acknowledgments
This work was funded by the project PID2019-105796GB-100/AEI/10.13039/501100011033 (Agencia Estatal de Investigación, Spain). M. Calvo-Rathert acknowledges funding from the Fulbright Commission and the Spanish Ministry of Science, Innovation, and Universities for a research stay at Hawaii University at Manoa. A. Goguitchaichvili acknowledges financial support from UNAM-PAPIIT no. IN101920. N. García-Redondo acknowledges financial support from Junta de Castilla y León and the European Research Development Fund (ERDF). EHB acknowledges financial support for laboratory maintenance and measurements to SOEST-HIGP and National Science Foundation grants. These is SOEST 11143 and HIGP 2420 contribution. The authors wish to thank Valera Shcherbakov and three anonymous reviewers, as well as editor Isabelle Manighetti for their constructive and helpful critics and comments, which greatly helped to improve the original text.

References

Adamia, S., Zakariadze, G., Chkhotua, T., Sadradze, N., Tsereteli, N., Chabukiani, A., & Gventsadze, A. (2011). Geology of the Caucasus: A review. *Turkish Journal of Earth Sciences*, *20*, 489–544. https://doi.org/10.3906/yer-1005-11

Adamia, S. A., Javakhishvili, S. I., & Zesashvili, V. I. (1960). Geological map of the USSR. Caucasian series. Scale 1/50000. Worksheets K-38-89G, K-38-90V. // Final geological report of the Mashavera geological-exploration unit and Geological expedition in South-Eastern Georgia, 1956–1959. Tbilisi, *GeolGruzUpravlenie* (in Russian).

Asanidze, B. Z., Adamiya, S. A., Tabagua, I. A., & Odikadze, N. S. (2009). The territory of Georgia and surrounding countries in the upper Cretaceous: Paleomagnetic data. *Izvestiya-Physics of the Solid Earth*, *45*(7), 42–53.

Aydinçakir, E., & Şen, C. (2013). Petrogenesis of the post-collisional volcanic rocks from the Borçka (Artvin) area: Implications for the evolution of the Eocene magmatism in the Eastern Pontides (NE Turkey). *Lithos*, *172*, 98–117.

Bazhenov, M., & Burtman, V. (2002). Eocene paleomagnetism of the Caucasus (southwest Georgia): Oroclinal bending in the Arabian syntaxis. *Tectonophysics*, *344*, 247–259.

Bazhenov, M. L., Burtman, V. S., & Levashova, N. L. (1996). Lower and Middle Jurassic paleomagnetic results from the south Lesser Caucasus and the evolution of the Mesozoic Tethys ocean. *Earth and Planetary Science Letters*, *141*, 79–89.

Besse, J., & Courtillot, V. (2002). Apparent and true polar wander and the geometry of the geomagnetic field over the last 200 Myr. *Journal of Geophysical Research*, *107*(B11), 2300. https://doi.org/10.1029/2000JB000050

Biggin, A., & Paterson, G. (2015). A new set of qualitative reliability criteria to aid inferences on paleomagnetic dipole moment variations through geological time. *Frontiers of Earth Science*, *2*, 24. https://doi.org/10.3389/feart.2014.00024

Biggin, A., & Poidras, T. (2006). First-order symmetry of weak field partial thermoremanence in multidomain ferromagnetic grains. 1. Experimental evidence and physical implications. *Earth and Planetary Science Letters*, *245*, 438–453. https://doi.org/10.1016/j.epsl.2006.02.035

Biggin, A. J., McCormack, A., & Roberts, A. (2010). Paleointensity database updated and upgraded. *Eos, Transactions American Geophysical Union*, *91*(2), 15. https://doi.org/10.1029/2010EO020003

Biggin, A. J., Strick, G. H. M., & Langereis, C. G. (2009). The intensity of the geomagnetic field in the late-Archaean: New measurements and an analysis of the updated IAGA paleointensity database. *Earth Planets and Space*, *61*, 9–22.

Bloemendal, J., King, J. W., Hall, F. R., & Doh, S. J. (1992). Rock magnetism of late Neogene and Pleistocene deep-sea sediments: Relationship of sediment source, diagenetic processes and sediment lithology. *Journal of Geophysical Research*, *97*, 4361–4375.

Böhnel, H. M., Dekkers, M. J., Delgado-Argote, L. A., & Gratton, M. N. (2009). Comparison between the microwave and the multispecimen partial difference pTRM paleointensity methods. *Geophysical Journal International*, *17*(2), 383–394.

Bowles, J. A., Jackson, M. J., Berquó, T. S., Sølheid, P. A., & Gee, J. S. (2013). Inferred time- and temperature-dependent cation ordering in natural titanomagnetites. *Nature Communications*, *4*, 1916. https://doi.org/10.1038/ncomms2938

Caccavari, A., Calvo-Rathert, M., Gogitchaichvili, A., He, H., Vashakidze, G., & Vegas, N. (2014). Paleomagnetism of the 40Ar/39Ar age of a Pliocene lava flow sequence in the Lesser Caucasus: Record of a clockwise rotation and analysis of paleosecular variation. *Geophysical Journal International*, *197*, 1354–1370.

Calvo-Rathert, M., Bógalo, M. F., Goguitchaichvili, A., Sologashvili, J., & Vashakidze, G. (2013). New paleomagnetic and paleointensity data from Pliocene lava flows from the Lesser Caucasus. *Journal of Asian Earth Sciences*, *73*, 347–361.

Calvo-Rathert, M., Bógalo, M. F., Morales, J., & Goguitchaichvili, A. (2020). Rock-magnetic, paleomagnetic and multimethod paleointensity Cretaceous and Paleogene lavas from the lesser Caucasus. http://doi.org/10.5281/zenodo.3997235.

Calvo-Rathert, M., Goguitchaichvili, A., Bógalo, M. F., Vegas-Tubía, N., Carrancho, A., & Sologashvili, J. (2011). A paleomagnetic and paleointensity study on Pleistocene and Pliocene basaltic flows from the Djavakheti Highland (Southern Georgia, Caucasus). *Physics of the Earth and Planetary Interiors*, *187*, 212–224.

Calvo-Rathert, M., Gogichaishvili, A., Vashakidze, G., & Sologashvili, J. (2015). New paleomagnetic and paleointensity data from Georgia (Caucasus): A review. *Latinmag Letters*, *5*(5), 1–22.

Calvo-Rathert, M., Goguichaichvili, A., Sologashvili, D., Villalaín, J. J., Bógalo, M. F., Carrancho, A., & Maissuradze, G. (2008). New paleomagnetic data from the hominin bearing Dmanisi paleo-anthropologic site (southern Georgia, Caucasus). *Quaternary Research*, *69*, 91–96.

Calvo-Rathert, M., Morales-Contreras, J., Carrancho, Á., Camps, P., Goguitchaichvili, A., & Hill, M. J. (2019). Reproductibility of archaeointensity determinations with a multimethod approach on archaeological material reproductions. *Geophysical Journal International*, *218*, 1719–1738. https://doi.org/10.1093/gji/ggz246

Calvo-Rathert, M., Morales-Contreras, J., Carrancho, Á., & Goguitchaichvili, A. (2016). A comparison of Thellier-type and multispecimen paleointensity determinations on Pleistocene and historical lava flows from Lanzarote (Canary Islands, Spain). *Geochemistry, Geophysics, Gecosystems*, *17*, 3638–3654. https://doi.org/10.1002/2016GC006396

Calvo-Rathert, M., Prévot, M., Perrin, M., & Riisager, J. (2002). Investigating the reasons for the failure of paleointensity experiments: A study on historical lava flows from Mt. Etna. *Geophysical Journal International*, *149*, 44–63.

Camps, P., Ruffet, G., Scherbakov, V., Scherbakova, V. V., Prévot, M., Moussine-Pouchkin, A., et al. (1996). Paleomagnetic and geochronological study of a geomagnetic field reversal or excursion recorded in Pliocene volcanic rocks from Georgia (Lesser Caucasus). *Physics of the Earth and Planetary Interiors*, *96*, 41–59.

Cande, S. C., & Kent, D. V. (1995). Revised calibration of the geomagnetic polarity timescale for the Late Cretaceous and Cenozoic. *Journal of Geophysical Research*, *100*, 6093–6095.

Chadima, M., & Hrouda, F. (2006). Remasoft 3.0 a user friendly paleomagnetic data browser and analyzer. *Travaux Géophysiques*, *XXVII*, 20–21.

Coe, R., Grommé, S., & Mankinen, E. A. (1978). Geomagnetic paleointensities from radiocarbon-dated lava flows on Hawaii and the question of the Pacific nondipol low. *Journal of Geophysical Research*, *83*, 1740–1756.

Constable, C., Tauxe, L., & Parker, R. L. (1998). Analysis of 11 Myr of geomagnetic intensity variation. *Journal of Geophysical Research*, *103*, 17735–17748.

Day, R., Fuller, M., & Schmidt, V. A. (1977). Hysteresis properties of titanomagnetites: Grain-size and compositional dependence. *Physics of the Earth and Planetary Interiors*, *13*, 260–267.

De Groot, L. V., Béguin, A., Kosters, M. E., van Rijsingen, M., Struijk, E. L. M., Biggin, A. J., et al. (2015). High paleointensities for the Canary Islands constrain the Levant geomagnetic high. *Earth and Planetary Science Letters*, *419*, 154–167. https://doi.org/10.1016/jepsl.2015.03.020

De Groot, L. V., Biggin, A. J., Dekkers, M. J., Langereis, C. G., & Herrero Bervera, E. (2013). Rapid regional perturbations to the recent global geomagnetic decay revealed by a new Hawaiian record. *Nature Communications*, *4*, 2727. https://doi.org/10.1038/ncomms3727

Dekkers, M. J., & Böhnel, H. N. (2006). Reliable absolute palaeointensities independent of magnetic domain state. *Earth and Planetary Science Letters*, *284*, 508–517.

Demarest, H. H. (1983). Error analysis for the determination of tectonic rotation from paleomagnetic data. *Journal of Geophysical Research*, *88*(B5), 4321–4328. https://doi.org/10.1029/JB088iB05p04321

Draeger, U., Prévot, M., Poidras, T., & Riisager, J. (2006). Single-domain chemical, thermochemical and thermal remanences in a basaltic rock. *Geophysical Journal International*, *166*, 12–32. https://doi.org/10.1111/j.1365-246X.2006.02862.x

Dudauri, O. Z., Vashakidze, G. T., & Gogoladze, D. P. (1990). K-Ar age of some hypabyssal bodies and ore deposits in Kvemo-Kartli (South-Eastern Georgia). *Proceedings of Georgian Academy of Sciences*, *140*(3), 553–556 (in Russian).

Dunlop, D. (2002). Theory and application of the Day plot (Mrs/Ms versus Hcr/Hc) 1. Theoretical curves and tests using titanomagnetite data. *Journal of Geophysical Research*, *107*(B3). 2056. https://doi.org/10.1029/2001JB000486

Dunlop, D. J. (2011). Physical basis of the Thellier-Thellier and related paleointensity methods. *Physics of the Earth and Planetary Interiors*, *187*, 118–138.

Enterpinar, P., Langereis, C. G., Biggin, A. J., de Groot, L. V., Kulakoğlu, F., Osmura, S., & Süel, A. (2016). Full vector archaeomagnetic records from Anatolia between 2400 and 1350 BCE: Implications for geomagnetic field models and the dating of fires in antquity. *Earth and Planetary Science Letters*, *434*, 171–186.

Fabian, K. (2003). Some additional parameters to estimate domain state from isothermal magnetization measurements. *Earth and Planetary Science Letters*, *213*, 337–345.

Fabian, K., & Leonhardt, R. (2010). Multi-specimen absolute paleointensity determination: An optimal protocol including pTRM normalization, domain-state correction and alteration test. *Earth and Planetary Science Letters*, *297*, 84–94.

Gogichaishvili, A., Caccavari, A., Calvo-Rathert, M., Morales, J., Vashakidze, G., He, H., & Vegas, N. (2016). Absolute paleointensity study of a pliocene lava flow sequence in the Lesser Caucasus just before Matuyama-Olduvay transition. *Physics of the Earth and Planetary Letters*, *257*, 158–170. https://doi.org/10.1016/j.pepi.2016.06.002

Gogichaishvili, A., Calvo-Rathert, M., Sologashvili, D., Alva Valdivia, L., & Urrutia-Fucugauchi, J. (2000). Paleomagnetic study of the Georgian Plio-Quaternary Volcanic Provinces (Southern Caucasus): A pilot study. *Comptes rendus de l'Académie des Sciences, Paris*, *11*, 331–336.

Gogichaishvili, A., Calvo-Rathert, M., Sologashvili, D., Morales, J., Soler, A. M., & Espinosa, M. (2001). A reconnaisance magnetostratigraphy of Georgian Plio-Quaternary Volcanic Provinces (Southern Caucasus). *Geofisica Internacional*, *40*, 111–119.

Goguitchaichvili, A., Cervantes, M. A., Calvo-Rathert, M., Camps, P., Sologashvili, J., & Maissuradze, G. (2009). Gilbert-Gauss geomagnetic reversal recorded in Pliocene volcanic sequences from Lesser Caucasus: Revisited. *Earth Planets and Space*, *61*, 71–82.

Goguitchaichvili, A., & Parès, J. M. (2000). A recognition paleomagnetic study of volcanic and sedimentary rocks from Dmanisi (Caucasus): Implications for the oldest human occupation in Europe. *Comptes rendus de l'Académie des Sciences, Paris*, *331*, 183–186.

Goguitchaichvili, A., Sologachvili, D., Prévot, M., Calvo, M., Pavlenchvili, E. S. H., Maissuradze, G. M., & Schnepp, E. (1997). Paleomagnetic and rock-magnetic study of a Pliocene volcanic section in South Georgia (Caucasus). *Geologie en Mijnbouw*, *76*, 135–143.

Gribov, S. K., Shcherbakov, V. P., & Aphinogenova, N. A. (2019). Magnetic properties of artificial CRM created on titanomagnetite-bearing oceanic basalts. In D. Nurgaliev, V. Shcherbakov, A. Kosterov, & S. Spassov (Eds.), *Recent advances in rock magnetism, environmental magnetism and paleomagnetism. Springer Geophysics. Cham: Springer*.

Grommé, C. S., Wright, T. L., & Peck, D. L. (1969). Magnetic properties and oxidation of iron-titanium oxide minerals in Alae and Makaopuhi lava lakes, Hawaii. *Journal of Geophysical Research*, *74*, 5277–5249.

He, H. Y., Pan, Y. X., Tauxe, L., Qin, H. F., & Zhu, R. X. (2008). Toward age determination of the M0r (Barremian-Aptian boundary) of the Early Cretaceous. *Physics of the Earth and Planetary Interiors*, *169*, 41–48.

Juárez, M. T., Tauxe, L., Gee, J. S., & Pick, T. (1998). The intensity of the Earth's magnetic field over the past 160 million years. *Nature*, *394*, 878–881. https://doi.org/10.1038/29746

Kirschvink, J. L. (1980). The least-square line and plane and the analysis of paleomagnetic data. *Geophysical Journal of the Royal Astronomical Society*, *62*, 699–718.

Koçyiğit, A., Yilmaz, A., Adamia, S., & Kuloshvili, S. (2001). Neotectonics of East Anatolian plateau (Turkey) and Lesser Caucasus: Implication for transition from thrusting to strike-slip faulting. *Geodinamica Acta*, *14*, 177–195.

Kulakov, E. V., Sprain, C. J., Doubrovine, P. V., Smirnov, A. V., Paterson, G. A., Hawkins, L., et al. (2019). Analysis of an updated paleointensity database (Q_{PI}-PINT) for 65-200 Ma: Implications for the long-term history of dipole moment through the Mesozoic. *Journal of Geophysical Research: Solid Earth*, *124*, 9999–10022. https://doi.org/10.1029/2018JB017287

Lebedev, V. A., Arakelyants, M. M., Gol'tsman, Y. V., & Oleinikova, T. I. (1999). Geochronology of magmatism, rock alteration, and ore deposition at the Verkhneurmiisk ore field (Khabarovskii krai, Russia). *Geology of Ore Deposits*, *41*(1), 61–72.

Leonhardt, R. (2006). Analyzing rock magnetic measurements: The RockMagAnalyzer 1.0 software. *Computers and Geosciences*, *32*, 1420–1431.

Leonhardt, R., Heunemann, C., & Krása, D. (2004). Analyzing absolute paleointensity determinations: Acceptance criteria and the software ThellierTool4.0. *Geochemistry, Geophysics, Gecosystems*, *5*, Q12016. https://doi.org/10.1029/2004GC000807

Leonhardt, R., Hufenbecher, F., Heider, F., & Soffel, H. (2000). High absolute paleointensity during a mid Miocene excursion of the Earth's magnetic field. *Earth and Planetary Science Letters*, *184*(1), 141–154. https://doi.org/10.1016/S0012-821X(00)00311-3.

Lordkipanidze, M., Meliksetian, B., & Djrbashian, R. (1989). Mesozoic-Cenozoic magmatic evolution of the Pontian-Crimean-Caucasian region. IGCP Project 198: Evolution of the Northern Margin of the Tethys. *Memoires de la Societé Géologique de France, Paris*, *154*, 101–124.

McFadden, P. L., & McElhinny, M. W. (1988). The combined analysis of remagnetisation circles and direct observations in paleomagnetism. *Earth and Planetary Science Letters*, *87*, 161–172.

Meijers, M. J. M., Smith, B., Pastor-Galán, D., Degenaar, R., Sadradze, N., Adamia, S., et al. (2015). Progressive orocline formation in the Eastern Pontides–Lesser Caucasus. Geological Society, London, Special Publications, *428*, 117–143. https://doi.org/10.1144/SP428.8

Michalk, D., Muxworthy, A. R., Böhnel, H., MacLennan, J., & Nowaczyk, N. R. (2008). Evaluation of the multispecimen parallel differential pTRM method: A test on historical lavas from Iceland and Mexico. *Geophysical Journal International*, *173*, 409–420.

Michalk, D. M., Biggin, A. J., Knudsen, M. F., Böhnel, H. N., Nowaczyk, N., Ownby, S., & López-Martínez, M. (2010). Application of the multispecimen paleointensity method to Pleistocene lava flows from the Trans-Mexican Volcanic Belt. *Physics of the Earth and Planetary Interiors*, *179*(3–4), 139–156.

Monster, M. W. L., de Groot, L. V., Biggin, A. J., & Dekkers, M. J. (2015a). The performance of various paleointensity techniques as a function of rock-magnetic behaviour—A case study for La Palma. *Physics of the Earth and Planetary Interiors*, *242*, 36–49.

Monster, M. W. L., de Groot, L. V., & Dekkers, M. J. (2015b). MSP-Tool: A VBA-based software tool for the analysis of multispecimen Paleointensity data. *Frontiers of Earth Science*, *3*, 86. https://doi.org/10.3389/feart.2015.00086

Monster, M. W. L., van Galen, J., Kuiper, K. F., Dekkers, M. J., & de Groot, L. V. (2018). A late-quaternary full-vector geomagnetic record from El Golfo section, El Hierro, Canary Islands. *Geophysical Journal International*, *215*, 1701–1717. https://doi.org/10.1093/gji/ggy361

Paterson, G., Tauxe, L., Biggin, A. J., Shaar, R., & Jonestrask, L. C. (2014). On improving the selection of Thellier-type paleointensity data. *Geochemistry, Geophysics, Gecosystems*, *15*, 1180–1192. https://doi.org/10.1002/2013GC005135

Pick, T., & Tauxe, L. (1994). Characteristics of magnetite in submarine basaltic glass. *Geophysical Journal International*, *119*, 116–128.

Prévot, M., Derder, M. E., McWilliams, M., & Thompson, J. (1990). Intensity of the Earth's magnetic field: Evidence for a Mesozoic dipole low. *Earth and Planetary Science Letters*, *97*, 129–139. https://doi.org/10.1016/0012-821X(90)90104-6

Rathert, M. C., Bógalo, M. F., Morales, J., & Gogichaishvili, A. (2020). *Rock-magnetic, paleomagnetic and multimethod paleointensity Cretaceous and Paleogene lavas from the lesser Caucasus*, https://doi.org/10.5281/zenodo.39.

Reilinger, R., McClusky, S., Vernant, P., Lawrence, S., Ergintav, S., Cakmak, R., et al. (2006). GPS constraints on continental deformation in the Africa-Arabia-Eurasia continental collision zone and implications for the dynamics of plate interactions. *Journal of Geophysical Research*, *111*, BO5411. https://doi.org/10.1029/2005JB004051

Riisager, J., Riisager, P., & Perrin, M. (1999). Palaeodirectional and palaeointensity results of Paleocene and Eocene basalts from West Greenland. *Bulletin of the Geological Society of Denmark*, *46*, 69–78.

Riisager, P., & Abrahamsen, N. (2000). Palaeointensity of West Greenland Palaeocene basalts: Asymmetric intensity around the C27n–C26r transition. *Physics of the Earth and Planetary Interiors*, *118*(1–2), 53–64.

Roberts, A. P., Tauxe, L., Heslop, D., Zhao, X., & Jiang, Z. X. (2018). A critical appraisal of the "Day Diagram". *Journal of Geophysical Research: Solid Earth*, *123*, 2618–2644. https://doi.org/10.1002/2017JB015247

Rolland, Y. (2017). Caucasus collisional history: Review of data from East Anatolia to West Iran. *Gondwana Research*, *49*, 130–146.

Sánchez-Moreno, E. M. (2018). *Variation of the absolute paleointensity of the Earth's magnetic field recorded in sequences of basaltic flows from the volcanic region of Djavakheti (Georgia) (PhD thesis*, 376 p.). Burgos, Spain: Universidad de Burgos. https://doi.org/10.13140/RG.2.2.30939.00804

Sánchez-Moreno, E. M., Calvo-Rathert, M., Goguitchaichvili, A., Tauxe, L., Vashakidze, G. T., & Lebedev, V. A. (2020). Weak paleointensity results over a Pliocene volcanic sequence from Lesser Caucasus (Georgia): Transitional record or time averaged field. *Geophysical Journal International*, *220*(3), 1604–1618. https://doi.org/10.1093/gji/ggz533

Sánchez-Moreno, E. M., Calvo-Rathert, M., Goguitchaichvili, A., Vashakidze, G. T., & Lebedev, V. A. (2018). Evidence of unusual geomagnetic regimes recorded in Plio-Pleistocene volcanic sequences from the Lesser Caucasus (Southern Georgia). *Geochemistry, Geophysics, Geosystems*, *19*, 1429–1446. https://doi.org/10.1029/2017GC007358

Selkin, A., & Tauxe, L. (2000). Long-term variations in paleointensity. *Philosophical Transactions of the Royal Society*, *358*, 1065–1088.

Shcherbakov, V. P., Gribov, S. K., Lhuillier, F., Aphinogenova, N. A., & Tsel'movich, V. A. (2019). On the reliability of absolute paleointensity determinations on basaltic rocks bearing a thermochemical remanence. *Journal of Geophysical Research*. *124*, 7616–7632. https://doi.org/10.1029/2019JB017873

Shcherbakova, V. V., Asanidze, B. Z., Shcherbakov, V. P., & Zhidkov, G. V. (2007). Geomagnetic field paleointensity in the Cretaceous from Upper Cretaceous rocks of Georgia. *Izvestiya-Physics of the Solid Earth*, *43*(11), 951–959.

Shcherbakova, V. V., Perrin, M., Shcherbakov, V. P., Pavlov, V. E., Ayvaz'yan, A., & Zhidkov, G. V. (2009). Rock magnetic and paleointensity results from Mesozoic baked contacts of Armenia. *Earth Planets and Space*, *61*, 23–39.

Smirnov, A. V., & Tarduno, J. A. (2005). Thermochemical remanent magnetization in Precambrian rocks: Are we sure the geomagnetic field was weak? *Journal of Geophysical Research*, *110*, B06103. https://doi.org/10.1029/2004JB003445

Steiger, R. H., & Jäger, E. (1977). Subcommission on geochronology: Convention on the use of decay constants in geo- and cosmochronology. *Earth and Planetary Science Letters*, *36*, 359–362.

Tarduno, J. A., & Cottrell, R. D. (2005). Dipole strength and variation of the time-averaged reversing and nonreversing geodynamo based on Thellier analyses of single plagioclase crystals. *Journal of Geophysical Research*, *110*, B11101. https://doi.org/10.1029/2005JB003970

Tauxe, L. (2006). Long-term trends in paleointensity: The contribution of DSDP/ODP submarine basaltic glass collections. *Physics of the Earth and Planetary Interiors*, *156*, 223–241. https://doi.org/10.1016/j.pepi.2005.03.022

Tauxe, L., Gee, J. S., Steiner, M. B., & Staudigel, H. (2013). Paleointensity results from the Jurassic: New constraints from submarine basaltic glasses of ODP Site 801C. *Geochemistry, Geophysics, Gecosystems*, *14*, 4718–4733. https://doi.org/10.1002/ggge.20282

Tauxe, L., & Pick, T. (1996). Potbellies, wasp-waists, and superparamagnetism in magnetic hysteresis. *Journal of Geophysical Research*, *101*, 571–583.

Thellier, E., & Thellier, O. (1959). Sur l'intensité du champ magnétique terrestre dans le passé historique et géologique. *Annales Geophysicae*, *15*, 285–376.

Walton, D., Shaw, J., Share, J., & Hakes, J. (1992). Microwave demagnetization. *Journal of Applied Physics*, *71*, 1549–1551.

Yilmaz, A., Adamia, S., Chabukiani, A., Chkhotua, T., Erdoğan, K., Tuzcu, S., & Karabiyikoğlu, M. (2000). Structural correlation of the southern Transcaucasus (Georgia)-eastern Pontides (Turkey). In E. Bozkurt, J. A. Winchester, & J. D. A. Piper (Eds.), Tectonics and magmatism in Turkey and the surrounding area (Vol. 173, pp. 171–182). London, UK: Geological Society, London, Special Publications.

Yu, Y., Tauxe, L., & Genevey, A. (2004). Toward an optimal geomagnetic field intensity determination technique. *Geochemistry, Geophysics, Geosystems*, *5*, Q02H07. https://doi.org/10.1029/2003GC000630.